Role of slow out-of-equilibrium modes on the dynamic structure factor near the QCD critical point

Golam Sarwar,[1,*] Md Hasanujjaman,[2,†] and Jan-e Alam[3,4,‡]

[1]*Theory Division, Physical Research Laboratory, Navrangpura, Ahmedabad 380 009, India*
[2]*Department of Physics, Darjeeling Government College, Darjeeling 734101, India*
[3]*Variable Energy Cyclotron Centre, 1/AF Bidhan Nagar, Kolkata 700064, India*
[4]*Homi Bhabha National Institute, Training School Complex, Mumbai 400085, India*

(Received 16 May 2022; accepted 6 October 2022; published 31 October 2022)

The role of slow out-of-equilibrium modes (OEMs), introduced to extend the validity of hydrodynamics near the QCD critical point on the power spectrum of dynamical density fluctuations has been studied. We have used the equation of motion of slow modes for the situation when the extensive nature of thermodynamics is not altered due to the introduction of the OEM. We find that the extensivity condition puts an extra constraint on the coupling of OEM with the 4-divergence of velocity. The dynamic structure factor $[\mathcal{S}_{nn}(\boldsymbol{k},\omega)]$ in the presence of the OEM shows four Lorentzian peaks asymmetrically positioned about $\omega(\text{frequency}) = 0$, whereas it shows three well-known Lorentzian peaks in the absence of the OEM. We find that the asymmetric peaks originate due to the coupling of the OEM with the hydrodynamic modes. It is also shown that the OEM has smaller effects on $\mathcal{S}_{nn}(\boldsymbol{k},\omega)$ evaluated within the scope of the first-order hydrodynamics (relativistic Navier-Stokes). The width of the Rayleigh peak is reduced in the presence of OEM, indicating the reduction of the decay rate of the fluctuations connected to the slowing down, a well-known characteristic of the critical end point.

DOI: 10.1103/PhysRevD.106.074029

I. INTRODUCTION

One of the outstanding issues in Relativistic Heavy Ion Collision experiments (RHIC-E) is to detect the critical end point (CEP) located at some critical baryonic chemical potential (μ_c) and critical temperature (T_c) in the QCD phase diagram. The existence of the CEP in QCD was suggested in Refs. [1–5] based on the effective field theoretic models and by lattice QCD simulations [6,7]. The experimental search for the CEP has been taken up through the beam energy scan program at the Relativistic Heavy Ion Collider [8]. The search for the CEP will continue in future experiments at the Facility for Anti-Proton and Ion Research and Nuclotron-Based Ion Collider Facility [9]. The exact location of the CEP is not known from the first principle because of the difficulties associated with the sign problem of the spin-half Dirac particle (quark) in lattice QCD calculations [10]. Some of the QCD based effective models such as Nambu-Jona-Lasinio and Polyakov loop extended Nambu-Jona-Lasinio predict the location of the CEP [2,5,11,12], but the results are dependent on the parameters of the models. However, the prediction of the location of the CEP is not the only problem. Even if the location of the CEP is predicted accurately, its experimental detection is extremely challenging because the measured quantities are affected by all the temperatures and densities through which the system passes: from the initial to the thermal freeze-out states, not only from the single point at (μ_c, T_c) of the phase diagram.

The space-time evolution of the fireball is studied by solving relativistic hydrodynamic equations controlling the conservation of the density of conserved quantities (energy, momentum, and net-baryon number). The hydrodynamics is used to describe the slowly evolving modes of the macroscopic system, while the faster nonhydrodynamic modes are set by the collision dynamics at the microscopic level. The time required to achieve local equilibrium is much shorter than the time required to attain global equilibrium. This separation of timescale is required for the applicability of hydrodynamics. The hydrodynamic modeling has been used to study the evolution of the fireball created in relativistic nuclear collisions with the inclusion of the CEP [13–16], although strictly speaking, it breaks down near the CEP [17] due to the divergence of the correlation length and enhanced fluctuations [18–20]. At the CEP, the correlation length diverges, resulting in the divergence of the timescale for local equilibration, which leads to the break down of the hydrodynamics. In other words, if the system encounters the CEP, then the correlation length (ξ) diverges, and the relaxation time which

*golamsarwar1990@gmail.com
†jaman.mdh@gmail.com
‡jane@vecc.gov.in

evolves as $\sim\xi^3$ also diverges, leading to critical slowing down [21–23]. Consequently, the system stays away from local thermal equilibrium, and the first-order (Navier-Stokes [24]) or the second-order [25] hydrodynamical model may become inapplicable. However, hydrodynamics can still be applied for systems far away from equilibrium by including the higher-order gradients of hydrodynamic fields. This is a very active field of contemporary research but beyond the scope of present work (we refer to Ref. [26] and references therein for details). The evolution of the order parameters for chiral (σ field) and deconfinement (Polyakov loop) phase transitions have been investigated by using the Langevin equation in the thermal background of quark and antiquark fluid near the CEP observing large wave length fluctuations and slowing down [27,28].

It has been shown in Ref. [17] that the validity of the hydrodynamics can be extended near CEP by introducing a slowly evolving scalar nonhydrodynamic field or the slow OEM, ϕ, which is subsequently incorporated in the definition of the entropy along with other hydrodynamical variables. The slow OEMs are not treated separately [17,29], as they are coupled with hydrodynamic modes.

It is important to point out here that the description of far-from-equilibrium conformal systems may converge to hydrodynamic evolution [30–34]. However, this may not be possible for general nonconformal systems [35,36] as the gradient expansion is not always convergent [37]. The above-mentioned gradient expansion of the hydrodynamic field may not be suitable for systems with large fluctuations near the CEP where the OEMs relax slowly. Instead, a separate treatment of these modes will allow us to avoid the problem of convergence of gradient expansion of hydrodynamic fields. The presence of slow modes and its coupling with different hydrodynamic fields allow the study of the fluctuations of large magnitudes near the CEP. In the present work, the role of ϕ on $\mathcal{S}_{nn}(\boldsymbol{k},\omega)$ will be studied using relativistic causal dissipative hydrodynamics proposed by Israel and Stewart (IS) [25]. The dispersion relations for the hydrodynamic modes are governed by the set of hydrodynamic equations, and the extensivity of thermodynamics restricts the coupling of slow modes with gradients of other hydrodynamic fields.

The fluctuations near the CEP in condensed matter system has been studied extensively. Specifically, the dynamic spectral structure [$\mathcal{S}_{nn}(\boldsymbol{k},\omega)$] has been investigated both experimentally and theoretically and found to be crucially dependent on the values of the various transport coefficients of the fluid [22,38,39]. According to the Onsager's hypothesis [40], the progression of thermally excited fluctuations is governed by the transport coefficients of the medium. The light and neutron scatterings experiments have been performed to investigate the properties of fluctuations experimentally in condensed matter physics. The spectrum of scattered light contains three identifiable peaks of Lorentzian distribution, a Rayleigh (R) peak [41], at angular frequency, $\omega = 0$, and two Brillouin (B) peaks located symmetrically in the opposite side of the R peak, experimentally detected by Fleury and Boon [42]. The R peak arises due to the entropy or temperature fluctuations at constant pressure, whereas B peaks arise from the pressure fluctuations at constant entropy. The width of the R peak is connected to the thermal conductivity (κ), isobaric specific heat (C_P), and the mass density of the fluid (ρ) as $\kappa/(\rho C_P)$ [22]. Therefore, if the order of divergence for κ is weaker than C_P, then a narrow R peak appears. Since the width represents the decay rate of the fluctuation, a narrow width will indicate the slower decay of fluctuation. The two B peaks are positioned at $\omega = \pm c_s k$ with respect to the frequency of the incident light, where c_s is the speed of sound and k is the wave vector. The finite width of the B peak provides information about the values of transport coefficients such as shear and bulk viscosities. The ratio of intensities of R peak to B peak is $I_R/2I_B = C_P/C_V - 1 = K_T/K_S - 1$, called the Landau-Placzek ratio, where K_T and K_S are isothermal and adiabatic compressibilities, respectively. As some of the transport coefficients and response functions change drastically, the study of the structure factor is very useful to understand the behavior of the fluid near the CEP where the B peaks tend to vanish, giving rise to severe modification in $\mathcal{S}_{nn}(\boldsymbol{k},\omega)$.

In QCD, however, no external probe exists to measure such a drastic change in $\mathcal{S}_{nn}(\boldsymbol{k},\omega)$. Nevertheless, it is a well-known feature of the critical phenomena that the behavior of a large class of systems near the CEP are independent of the dynamical details. Since the CEP in QCD belongs to same universality class, $\mathcal{O}(4)$ [1,4], as that of liquid-gas critical point, the role of such slow modes can be tested in liquid-gas system, and the knowledge gained can be very helpful to guide the theoretical modelling relevant to the CEP of QCD. In this context, the qualitative and quantitative effects of the slow modes on various physical quantities should be studied. In the present work, the effects of the slow modes on the spectral structure of the density fluctuations near the CEP [43,44] or more specifically the role of the slow modes on the Rayleigh and Brillouin peaks of $\mathcal{S}_{nn}(\boldsymbol{k},\omega)$ have been investigated. The static and dynamic structure factors have been estimated for QCD matter near CEP with stochastic diffusion dynamics of net baryon number in Refs. [45–47].

By definition of the critical point the quantity, $(\partial P/\partial V)_{\text{critical point}}$ approaches zero, leading to the divergence of the isothermal compressibility [$\kappa_T \sim (\partial V/\partial P)_T$] and hence resulting in a large fluctuation in density, as $\overline{(\delta n)^2} \propto \kappa_T$). This large fluctuation may reflect on experimental observables. Thermal fluctuations can cause entropy production, leading to fluctuation in multiplicity; however, their ensemble average is unaffected [48]. These fluctuations may not influence the lower flow harmonics but affect their correlation. Recently, CMS collaborations

have measured higher flow harmonics, which again carry a strong signature of thermal fluctuations [49], indicating that the measurement of fluctuations in multiplicity and higher harmonics as a function of collision energy at various rapidity bins may provide signal of CEP (see Ref. [50] for a recent review). An enhancement of event-by-event fluctuation in net proton due to the CEP has been observed in Ref. [51]. The explicit dependence of the correlation of the multiplicity fluctuation on the hydrodynamic properties (speed of sound and shear viscosity) of the fluid in rapidity space has been shown in Ref. [52] within the scope of longitudinally expanding system with boost invariance [53]. It will be interesting to study the same correlation with the inclusion of the CEP (as both the viscosity and speed of sound get affected by the CEP) by using full $(3+1)$-dimensional expansion within the ambit of relativistic second-order viscous hydrodynamics. The effects of out-of-equilibrium dynamics and space-time inhomogeneity on the kurtosis of net baryon and σ field containing the signal of CEP have been studied in Refs. [54].

The present paper is organized as follows. In the next section, i.e., in Sec. II, the expression for $\mathcal{S}_{nn}(\boldsymbol{k},\omega)$ will be derived by including the variable, ϕ, representing the nonhydrodynamic mode. In Sec. III, the results are presented, and Sec. IV is devoted to a summary and discussion.

II. HYDRODYNAMICS WITH OUT-OF-EQUILIBRIUM MODES

The evolution of fluid near the CEP within the scope of fluid dynamics can be extended by introducing an extra slow degree of freedom representing the soft mode [17]. For this purpose, we use the IS hydrodynamical model [25] in Eckart frame [55] to study the effects of this slow degree of freedom. The signature metric for the Minkowski space time is taken as $g^{\mu\nu}=(-1,1,1,1)$. The fluid velocity field, u^μ, is normalized as $u^\mu u_\mu=-1$.

The energy-momentum and charge (net baryon number here) conservation equations are, respectively,

$$\partial_\mu T^{\mu\nu}=0 \tag{1}$$

and

$$\partial_\mu J^\mu=0, \tag{2}$$

where

$$T^{\mu\nu}=\epsilon u^\mu u^\nu+(P+\Pi)\Delta^{\mu\nu}+h^\mu u^\nu+u^\mu h^\nu+\pi^{\mu\nu} \tag{3}$$

is the energy-momentum tensor and

$$J^\mu=nu^\mu+n^\mu \tag{4}$$

is the baryonic current. In Eq. (3), $q^\mu=h^\mu-n^\mu(\epsilon+P)/n$ is the heat flux; h^μ is the vector dissipation or dissipative energy flow; u^μ is the flow velocity, with $u_\mu h^\mu=u_\mu\pi^{\mu\nu}=0$; n is the conserved charge number density (net baryon density for RHIC-E); n^μ is dissipative current density; ϵ is energy density; P is the pressure; Π is the scalar dissipation or the bulk stress; $\pi^{\mu\nu}$ is the tensor dissipation or shear stress tensor; and $\Delta^{\mu\nu}=g^{\mu\nu}+u^\mu u^\nu$ is the projection operator, such that $\Delta^{\mu\nu}u_\nu=0$. In the Eckart frame, $n^\mu=0$, which leads to $q^\mu=h^\mu$.

The evolution can be studied by solving the hydrodynamic equations [Eqs. (1) and (2)] with the appropriate initial conditions and equation of state. However, the solution of these equations become invalid near the CEP. To extend the validity of the hydrodynamics near the CEP, a scalar field, ϕ, is introduced in the following way, and the resulting model is referred as hydro+ [17]. In hydro+ formalism, the partial equilibrium entropy gets separate contribution from the slow mode ϕ. The change in entropy density due to the introduction of the scalar field, ϕ, is given by

$$ds_+=\beta_+d\epsilon-\alpha_+dn-\pi d\phi, \tag{5}$$

where π is the "energy cost" for the addition of ϕ to the system and hence π can be called as the chemical potential corresponding to ϕ. Here, $\alpha_+=\mu_+/T$, where T is the temperature and μ_+ is the chemical potential. The relaxation equation for additional scalar soft mode, ϕ, is introduced as [17]

$$D\phi=-F_\phi+A_\phi\theta, \tag{6}$$

where $\theta=\partial_\mu u^\mu$ and $D=u^\mu\partial_\mu$. Forms of F_ϕ and A_ϕ can be obtained by imposing the second law of thermodynamics, which states

$$\partial_\mu s^\mu\geq 0, \tag{7}$$

where s^μ is the entropy four current and is defined as

$$s^\mu=su^\mu+\Delta s^\mu. \tag{8}$$

The role of the nonhydrodynamic mode on the extensivity condition has not been considered earlier to the best of our knowledge. In the present work, we find that the extensivity condition is important for determining the form of A_ϕ. For notational simplicity, we drop the subscript "+" from here onward and write the following relations as obtained from the extensivity condition discussed in Appendix A, in the presence of ϕ as

$$\beta dP=-(\epsilon+P)d\beta+nd\alpha+\phi d\pi, \tag{9}$$

$$s=\beta(\epsilon+P-\mu n)-\pi\phi. \tag{10}$$

The equation for the soft mode, Eq. (6), is already of relaxation type in its form; therefore, the coupling of slowly evolving soft modes at first order is adequate to

maintain causality. The coupling with the soft mode in first order can be achieved as

$$\partial_\mu s^\mu = (F_\phi - b\partial_\mu q^\mu)\pi - q^\mu\partial_\mu(\beta + b\pi) - \beta(\partial_\mu u_\nu)\Delta T^{\mu\nu} + \partial_\mu(\Delta s^\mu + \beta q^\mu + b\pi q^\mu) + S_n\theta, \tag{11}$$

where b represents the coupling strength between the slow mode and the heat flux, which is expected to modify the spectral function. The S_n is given by

$$S_n = s - \beta(\epsilon + P) + \mu\beta n + \pi A_\phi. \tag{12}$$

$\partial_\mu s^\mu \geq 0$ can be satisfied with redefinition of π, q^μ, $\Delta T^{\mu\nu}$, and s^μ; therefore, we have

$$\Delta s^\mu = -\beta q^\mu - b\pi q^\mu \tag{13}$$

and

$$q^\mu = -\kappa T\left[Du^\mu - \frac{1}{\beta}\Delta^{\mu\nu}\partial_\nu(\beta + b\pi)\right], \tag{14}$$

$$F_\phi = \gamma\pi - b\partial_\mu\left[\kappa T Du^\mu - \frac{\kappa}{\beta}\Delta^{\mu\nu}\partial_\nu(\beta + b\pi)\right], \tag{15}$$

where the proportionality constants $\kappa \geq 0$ and $\gamma \geq 0$ are, respectively, thermal conductivity and the relaxation rate of slow modes. Along with the above expression of fluxes, one also needs $S_n = c\theta$, with $c \geq 0$ being a constant to satisfy the relation $\partial_\mu s^\mu \geq 0$. However, since S_n contains local thermodynamic quantities at zeroth order in the derivative, it cannot be a function of the four divergence of fluid velocity, θ. In other words, the relation $S_n = c\theta$ with nonzero c will make the local equilibrium entropy density in the fluid rest frame a function of the dissipative gradient of the fluid velocity which is frame dependent. In that case, the local equilibrium entropy will be frame dependent, but the frame dependence of entropy is contradictory to its definition as a frame-independent quantity. So c should be zero, implying $S_n = 0$.

Comparison of Eqs. (10) and (12) gives $A_\phi = \phi$ for $S_n = 0$. Therefore, the modified expressions of fluxes in the second-order IS theory with the coupling to soft modes read as

$$\begin{aligned}
\Pi &= -\frac{1}{3}\zeta[\partial_\mu u^\mu + \beta_0 D\Pi - \tilde{\alpha}_0\partial_\mu q^\mu], \\
q^\mu &= -\kappa T\Delta^{\mu\nu}[\beta\partial_\nu(T + b\pi) + Du_\nu \\
&\quad + \beta_1 Dq_\nu - \tilde{\alpha}_0\partial_\nu\Pi - \tilde{\alpha}_1\partial_\lambda\pi^\lambda_\nu], \\
\pi^{\mu\nu} &= -2\eta[\Delta^{\mu\nu\rho\lambda}\partial_\rho u_\lambda + \beta_2 D\pi^{\mu\nu} - \tilde{\alpha}_1\Delta^{\mu\nu\rho\lambda}\partial_\rho q_\lambda],
\end{aligned} \tag{16}$$

with constants of proportionality $\eta \geq 0$, $\zeta \geq 0$, where η and ζ are the shear and bulk viscous coefficients, respectively, and $\Delta^{\mu\nu\rho\lambda} = \frac{1}{2}[\Delta^{\mu\rho}\Delta^{\nu\lambda} + \Delta^{\nu\rho}\Delta^{\mu\lambda} - \frac{2}{3}g^{\mu\nu}\Delta^{\rho\lambda}]$. The quantities $\tilde{\alpha_0}$ and $\tilde{\alpha_1}$ are coupling coefficients, and β_0, $\tilde{\beta_1}$, and β_2 are relaxation coefficients. The relations of β_0, β_1, and β_2 with the relaxation time scales are given by (see Refs. [56,57] for details):

$$\tau_\Pi = \zeta\beta_0, \qquad \tau_q = \kappa T\beta_1, \qquad \tau_\pi = 2\eta\beta_2. \tag{17}$$

The coupling coefficients, which couple the heat flux to the bulk pressure $(l_{q\Pi}, l_{\Pi q})$ and the heat flux to the shear tensor $(l_{q\pi}, l_{\pi q})$, are related to the relaxation lengths by the following relations:

$$l_{\Pi q} = \zeta\alpha_0, \quad l_{q\Pi} = \kappa T\alpha_0, \quad l_{q\pi} = \kappa T\alpha_1, \quad l_{\pi q} = 2\eta\alpha_1. \tag{18}$$

The expressions for relaxation and coupling coefficients are taken from Ref. [44].

A. Linearized equations and the dynamic structure factor

Next, we linearize the hydrodynamic equations for small deviations from equilibrium field quantities and solve in frequency (ω)-wave vector ($\boldsymbol{k}$) space to obtain the $\mathcal{S}_{nn}(\boldsymbol{k}, \omega)$. We assume $\mathcal{Q} = \mathcal{Q}_0 + \delta\mathcal{Q}$, where $\mathcal{Q}$, $\mathcal{Q}_0$, and $\delta\mathcal{Q}$ represent general hydrodynamic variables, their average values, and fluctuations, respectively (for pedagogical approach on hydrodynamic fluctuation, we refer to Ref. [58]). $\mathcal{Q}_0 = 0$ is its average value for dissipative degrees of freedom and $u_0^\mu = (-1, 0, 0, 0)$ and $\delta u^\mu = (0, \delta\boldsymbol{u})$. The expressions for Π, q^μ and $\pi^{\mu\nu}$ given in Eq. (16) have been substituted in Eq. (3) to obtained $T^{\mu\nu}$ and subsequently Eqs. (1) and (2) have been solved under linear approximation in $(\omega, \boldsymbol{k})$ space. In the linearized domain, the equations of motion for different space-time components of the energy-momentum tensor and baryonic charge current obtained from Eqs. (1) and (4) read as

$$0 = -\frac{\partial\delta\epsilon}{\partial t} - (\epsilon_0 + P_0)\boldsymbol{\nabla}\cdot\delta\boldsymbol{u} - \boldsymbol{\nabla}\cdot\delta\boldsymbol{q}, \tag{19a}$$

$$0 = -(\epsilon_0 + P_0)\frac{\partial}{\partial t}\delta u^i - \partial^i(\delta P + \delta\Pi) + \frac{\partial}{\partial t}\delta q^i - \partial_j\Pi^{ij}, \tag{19b}$$

$$0 = -\frac{\partial}{\partial t}\delta n - n_0\boldsymbol{\nabla}\cdot\delta\boldsymbol{u}, \tag{19c}$$

$$0 = \delta\Pi + \frac{1}{3}\zeta[\boldsymbol{\nabla}\cdot\delta\boldsymbol{u} + \beta_0\frac{\partial}{\partial t}\delta\Pi - \tilde{\alpha_0}\boldsymbol{\nabla}\cdot\delta\boldsymbol{q}], \tag{19d}$$

$$0 = \delta q^i + \kappa T_0\nabla^i\delta T + \kappa T_0\frac{\partial}{\partial t}\delta u^i + \kappa T_0\beta_1\frac{\partial}{\partial t}\delta q^i - \kappa T_0\tilde{\alpha}_0\nabla^i\delta\Pi - \kappa T_0\tilde{\alpha}_1\nabla_j\pi^{ij}, \tag{19e}$$

$$0 = \delta\pi^{ij} + 2\eta\delta^{ijlm}(\partial_l\delta u_m - \tilde{\alpha}_1\partial_l\delta q_m) + 2\eta\beta_2\frac{\partial}{\partial t}\delta\pi^{ij}, \tag{19f}$$

$$0 = -\frac{\partial}{\partial t}\delta\phi - \left(\gamma + T_0^2\frac{K_{q\pi}^2}{\kappa}\nabla^2\right)C_{\phi\pi}\delta\phi - \left[\gamma + \left(T_0^2\frac{K_{q\pi}^2}{\kappa} - \frac{K_{q\pi}}{C_{T\pi}}\right)\nabla^2\right]C_{T\pi}\delta T - \left(\gamma + T_0^2\frac{K_{q\pi}}{\kappa}\nabla^2\right)C_{\pi n}\delta n - T_0 K_{q\pi}\frac{\partial}{\partial t}(\nabla_i\delta u^i) + \phi\nabla_i\delta u^i, \tag{19g}$$

where $K_{q\pi} = b\kappa$ and

$$C_{A\pi} = \frac{\partial\pi}{\partial A}, \quad \text{with} \quad A \equiv (T, n, \phi). \tag{20}$$

We get a system of linear equations in $\omega - k$ space (Appendix B) by taking the Fourier transformation of the above sets of equations. The Fourier transform of $\delta Q(\boldsymbol{r}, t)$ denoted by $\delta\tilde{Q}(\boldsymbol{k}, \omega)$ is defined as

$$\delta\tilde{Q}(\boldsymbol{k}, \omega) = \int_{-\infty}^{\infty} d^3r \int_0^{\infty} dt e^{-i(\boldsymbol{k}\cdot\boldsymbol{r}+\omega t)}\delta Q(\boldsymbol{r}, t), \tag{21}$$

and the Fourier transform of $\delta Q(\boldsymbol{r}, t)$ at $t = 0$ is given by

$$\delta\tilde{Q}(\boldsymbol{k}, t = 0) = \int_{-\infty}^{\infty} d^3r \int_0^{\infty} e^{-i\boldsymbol{k}\cdot\boldsymbol{r}}\delta Q(\boldsymbol{r}, t = 0). \tag{22}$$

The set of relevant equations, Eqs. (B3)–(B13), is given in Appendix B and can be written in the matrix form as

$$\mathbb{M}\delta\mathcal{Q} = \mathcal{A}, \tag{23}$$

where $\mathbb{M}$ is an 11×11 matrix representing the coefficients of the column vector comprising the quantities $\delta n, \delta T, \delta u_{||}, \delta u_{\perp}, \delta\Pi, \delta q_{||}, \delta q_{\perp}, \delta\pi_{||||}, \delta\pi_{||\perp}, \delta\pi_{\perp\perp}$, and $\delta\phi$. For notational simplicity, the tilde sign on the functions will be ignored from here onward for all the Fourier transformed quantities, but this will not cause any confusion as the ω and k explicitly appear as the arguments of the relevant quantities.

The solution of the set of linear equations can be written as

$$\delta\mathcal{Q} = \mathbb{M}^{-1}\mathcal{A}. \tag{24}$$

In the present work, we are interested in evaluating the two-point correlation of density fluctuation. The solution of the set of equations represented by Eq. (24) leads to the following expression for density fluctuation (δn):

$$\begin{aligned}\delta n(\boldsymbol{k}, \omega) = {} & (-\epsilon_n\mathbb{M}_{12}^{-1} - \mathbb{M}_{11}^{-1})\delta n(\boldsymbol{k}, t = 0) + \epsilon_T(-\mathbb{M}_{12}^{-1})\delta T(\boldsymbol{k}, t = 0) + (-\epsilon_\phi\mathbb{M}_{12}^{-1} - \mathbb{M}_{13}^{-1})\delta\phi(\boldsymbol{k}, t = 0) \\ & + (\epsilon_0\mathbb{M}_{14}^{-1} - ikT_0\mathbb{M}_{13}^{-1}\kappa_{q\pi} + \mathbb{M}_{14}^{-1}P_0 - T_0\chi\mathbb{M}_{15}^{-1})\delta u_{||}(\boldsymbol{k}, t = 0) \\ & + (-\beta_1 T_0\chi\mathbb{M}_{15}^{-1} - \mathbb{M}_{14}^{-1})\delta q_{||}(\boldsymbol{k}, t = 0) + \frac{1}{3}\zeta\mathbb{M}_{16}^{-1}\beta_0\delta\pi(\boldsymbol{k}, t = 0) - 2\eta\mathbb{M}_{17}^{-1}\beta_2\delta\pi_{||||}(\boldsymbol{k}, t = 0) \\ & - 2\eta\mathbb{M}_{18}^{-1}\beta_2\pi_{\perp\perp}(\boldsymbol{k}, t = 0) + (\epsilon_0\mathbb{M}_{19}^{-1} + \mathbb{M}_{19}^{-1}P_0 - T_0\chi\mathbb{M}_{110}^{-1})\delta u_{\perp}(\boldsymbol{k}, t = 0) \\ & + (-\beta_1 T_0\chi\mathbb{M}_{110}^{-1} - \mathbb{M}_{19}^{-1})\delta q_{\perp}(\boldsymbol{k}, t = 0) - 2\eta\mathbb{M}_{111}^{-1}\beta_2\delta\pi_{||\perp}(\boldsymbol{k}, t = 0),\end{aligned} \tag{25}$$

where $\epsilon_x = \frac{\partial\epsilon}{\partial x}$ and $x = n, T, \phi$.

Now, we define the correlation of density fluctuations [22], $\mathcal{S}'_{nn}(\boldsymbol{k}, \omega)$ as follows:

$$\mathcal{S}'_{nn}(\boldsymbol{k}, \omega) = \langle\delta n(\boldsymbol{k}, \omega)\delta n(\boldsymbol{k}, 0)\rangle. \tag{26}$$

$\mathcal{S}'_{nn}(\boldsymbol{k}, \omega)$ can be calculated by substituting the expression for δn given by Eq. (25) in Eq. (26).

The correlation between two independent thermodynamic variables, say, $\mathcal{Q}_i$ and $\mathcal{Q}_j$, vanishes; i.e., we have

$$\langle\delta\mathcal{Q}_i(\boldsymbol{k}, \omega)\delta\mathcal{Q}_j(\boldsymbol{k}, t = 0)\rangle = 0, \quad i \neq j. \tag{27}$$

Therefore, the terms like $< \delta u_{||}\delta q_{||} >$, etc., will not contribute to $\mathcal{S}'_{nn}(\boldsymbol{k}, \omega)$,

$$\mathcal{S}'_{nn}(\boldsymbol{k}, \omega) = -\left[\left(\frac{\partial\epsilon}{\partial n}\right)\mathbb{M}_{12}^{-1} - \mathbb{M}_{11}^{-1}\right] \times \langle\delta n(\boldsymbol{k}, t = 0)\delta n(\boldsymbol{k}, t = 0)\rangle. \tag{28}$$

It may be noted that the elements $\mathbb{M}_{12}$ and $\mathbb{M}_{11}$ provide nonzero contributions to $\mathcal{S}'_{nn}$ and contributions for all other elements are zero because of the condition imposed by Eq. (27). The final expression for the $\mathcal{S}_{nn}(\boldsymbol{k}, \omega)$ can be obtained as

$$\mathcal{S}_{nn}(\boldsymbol{k}, \omega) = \frac{\mathcal{S}'_{nn}(\boldsymbol{k}, \omega)}{\langle\delta n(\boldsymbol{k}, t = 0)\delta n(\boldsymbol{k}, t = 0)\rangle} = -\left[\left(\frac{\partial\epsilon}{\partial n}\right)\mathbb{M}_{12}^{-1} - \mathbb{M}_{11}^{-1}\right]. \tag{29}$$

This is the correlation in density fluctuation or the power spectrum with the inclusion of the extra degree of freedom, ϕ.

III. RESULTS AND DISCUSSION

The aim of this work is to find out the spectral structure of density fluctuation within the scope of relativistic causal hydrodynamics with its validity extended near the CEP by introducing a scalar field as discussed above. The effect of the CEP is taken into consideration through an equation of state (EOS), containing the critical point. The EOS is constructed from the universality hypothesis, which suggests that the CEP of the QCD belongs to same universality class as the three-dimensional (3D) Ising model. We do not repeat the discussion on the construction of the EOS here but refer to the appropriate literature [16,44,59,60] for details. The behavior of various transport coefficients and response functions plays a crucial role in determining the structure factor in the presence of the CEP. The scaling behavior of various transport coefficients and thermodynamic functions near the CEP has been taken into account by using the following relations [61–63]:

$$\kappa_T = \kappa_T^0 |r|^{-\gamma'}, \quad C_V = C_0 |r|^{-\alpha}, \quad C_P = \frac{\kappa_0 T_0}{n_0}\left(\frac{\partial P}{\partial T}\right)_n^2 |r|^{-\gamma'},$$
$$c_s^2 = \frac{T_0}{n_0 h_0 C_0}\left(\frac{\partial P}{\partial T}\right)_n^2 |r|^{\alpha}, \quad \alpha_p = \kappa_0 \left(\frac{\partial P}{\partial T}\right)_n |r|^{-\gamma'}$$
$$\eta = \eta_0 |r|^{1+a_\kappa/2-\gamma'}, \quad \zeta = \zeta_0 |r|^{-a_\zeta}, \quad \kappa = \kappa_0 |r|^{-a_\kappa}, \quad (30)$$

where $r = (T - T_c)/T_c$ is the reduced temperature and α, γ', a_ζ, and a_κ are the critical exponents. Here, $\alpha = 0.11$ and $\gamma' = 1.2$. We take the values $a_\zeta = \nu d - \alpha = 1.78$ (here, $d = 3$, $\nu = 0.63$), and $a_\kappa = 0.63$. The partial derivative, $(\frac{\partial P}{\partial T})_n$, has been evaluated by using the EOS for consistency.

The critical behaviors of the second-order coupling and relaxation coefficients of the IS hydrodynamics have also been taken into account here (see Ref. [44] for details). To discern the effect of the scalar field ϕ on $\mathcal{S}_{nn}(\boldsymbol{k}, \omega)$, first we discuss the profile of $\mathcal{S}_{nn}(\boldsymbol{k}, \omega)$ in the absence of ϕ for two scenarios: when the system is (i) away from the CEP and (ii) near the CEP. For the first, it is well known that in the absence of ϕ the $\mathcal{S}_{nn}(\boldsymbol{k}, \omega)$ has three well-known peaks. These are the R peak located at $\omega = 0$ (due to entropy fluctuation at constant pressure) and the B peaks located symmetrically on either side of the R peak (due to pressure fluctuation at constant entropy). For the second, the $\mathcal{S}_{nn}(\boldsymbol{k}, \omega)$ shows a single peak at $\omega = 0$, and the B peaks vanish due to vanishing of sound speed in systems near the CEP [44].

This profile of $\mathcal{S}_{nn}(\boldsymbol{k}, \omega)$ is different from the one discussed above when the field ϕ is introduced. The locations of the four peaks of $\mathcal{S}_{nn}(\boldsymbol{k}, \omega)$ for different values of ω are obtained from the dispersion relation provided in the Appendix C. In Fig. 1(a), the variation of $\mathcal{S}_{nn}(\boldsymbol{k}, \omega)$ with ω for nonzero ϕ is shown for $k = 0.1$ fm^{-1} when the system is away from the CEP. The $\mathcal{S}_{nn}(\boldsymbol{k}, \omega)$ admits four peaks in the presence of ϕ. It is interesting to note that there is no elastic peak (R peak) at $\omega = 0$. The two away side peaks are identified as the B peaks corresponding to the Stokes (left side) and the anti-Stokes components (right side) located asymmetrically on either side of the origin with unequal peak heights. The asymmetry in the B peaks may arise due to the local inhomogeneity present in the system. The B peaks arise from propagating sound modes associated with pressure fluctuations at constant entropy. In condensed matter physics, the asymmetry of the B peaks is understood from the fact that two sound modes with different ω values, $\pm c_s k$, originate from different temperature zones [64,65]. The other two peaks (closer to $\omega = 0$) are present even with vanishing speed of sound in the

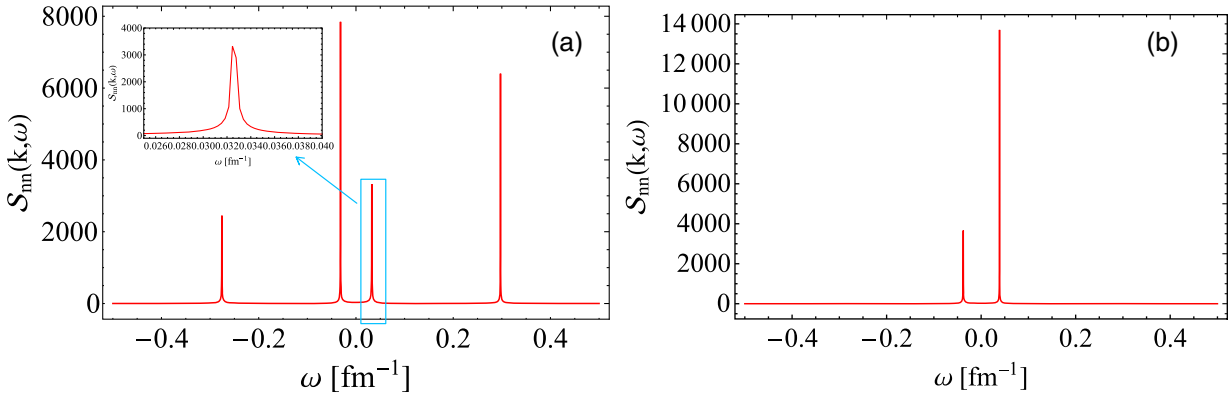

FIG. 1. (a) Variation of $\mathcal{S}_{nn}(\boldsymbol{k}, \omega)$ with ω for $k = 0.1$ fm^{-1} and $\eta/s = \zeta/s = \kappa T/s = 1/4\pi$, when the system is away from CEP ($r = 0.2$). The peaks are appearing as very narrow due to the scale chosen along x axis, and the change in the x-axis scale makes the width visible (see the inset for the R peak). (b) The system is close to the CEP ($r = 0.01$). The results are obtained with the equation of state containing the CEP and the transport coefficients, and the thermodynamic response function and the relaxation coefficients are estimated from the scaling behavior.

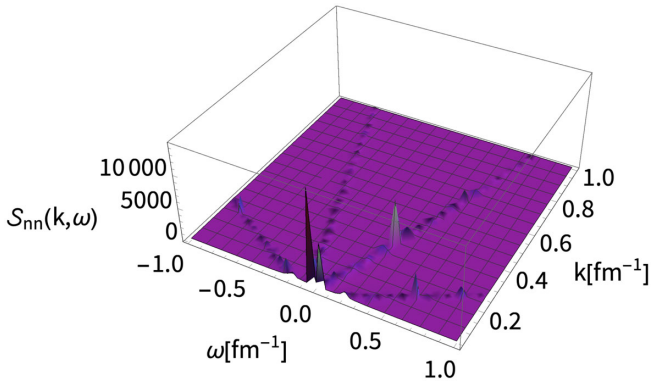

FIG. 2. Variation of $\mathcal{S}_{nn}(\boldsymbol{k},\omega)$ with ω and k for $r = 0.2$, i.e., when the system is away from CEP.

neighborhood of the CEP [as shown in Fig. 1(b)], arising due to the coupling of ϕ with q^{μ}. The coupling of ϕ with the hydrodynamical fields has resulted in one extra peak and the shifting of the R peak from $\omega = 0$. The peak appears at $\omega = 0$ for static thermal fluctuations (without time variation) on the magnitude of the fluctuations. Their appearance at nonzero ω represents the variation in the magnitude of the fluctuation with time. So, the appearance of these peaks at $\omega \neq 0$ (instead of at $\omega = 0$) is due to the time varying thermal fluctuations. The time variation in thermal fluctuation is due to the coupling of the heat flux to slow nonequilibrium modes. The slow nonequilibrium modes have much slower dynamic evolution rate, so thermal fluctuations become time dependent instead of being time independent. A nonrelativistic fluid system placed in a stationary temperature gradient showed asymmetry between Stokes and anti-Stokes components, and the asymmetry is maximum when $k||\nabla T$ and vanishes with $k\perp\nabla T$. The asymmetry present in Rayleigh component is exactly opposite to the Brillouin components. In the vicinity of the CEP (right panel), the $\mathcal{S}_{nn}(\boldsymbol{k},\omega)$ shows

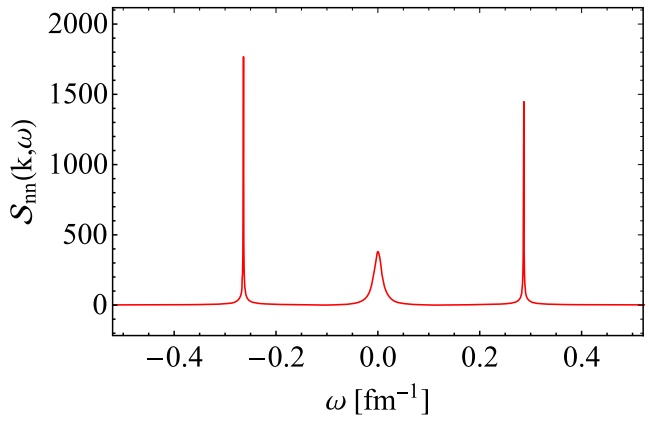

FIG. 3. Variation of $\mathcal{S}_{nn}(\boldsymbol{k},\omega)$ with ω for $k = 0.1$ fm^{-1} and $r = 0.2$, i.e., when the system is away from CEP for $K_{q\pi} = 0$.

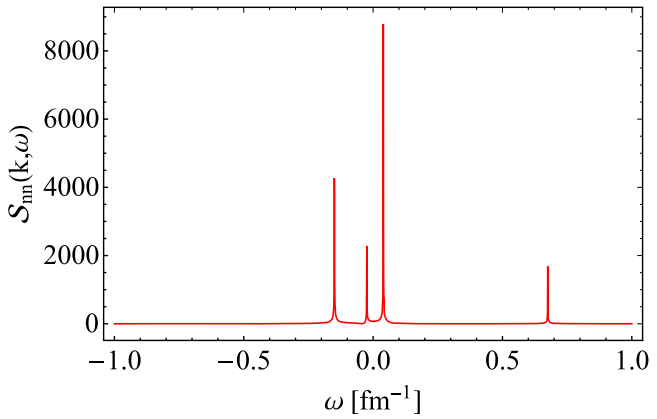

FIG. 4. Variation of $\mathcal{S}_{nn}(\boldsymbol{k},\omega)$ with ω for $k = 0.1$ fm^{-1} and $r = 0.2$, i.e., the system is away from CEP but with higher value of $(\frac{\partial P}{\partial \phi})$. The asymmetry in the B peaks is clearly visible.

two peaks closer to $\omega = 0$ as the B peaks disappear due to the absorption of sound at the CEP.

In Fig. 2, the structure factor in the ω-k plane is plotted when the system is away from CEP. The structure of $\mathcal{S}_{nn}(\boldsymbol{k},\omega)$ with nonzero ϕ is quite different from the case when $\phi = 0$. In case of $\phi = 0$, there will be a R peak and two B peaks with diminishing heights with the increase of k values. However, with $\phi \neq 0$, there are peaks appear at nonzero ω and k values due to the coupling of ϕ with other hydrodynamic fields. The structure of $\mathcal{S}_{nn}(\boldsymbol{k},\omega)$ with R and B peaks can be reproduced when the coupling of π (the chemical potential corresponding to the variable ϕ) with flux q is set to zero (Fig. 3).

The quantity, $\partial P/\partial\phi$, is connected to the fluctuation of ϕ as $\overline{(\Delta\phi)^2} \propto \phi^{-1}(\partial P/\partial\phi)^{-1}$ in analogy with $\overline{(\Delta n)^2} \propto n^{-1}(\partial P/\partial n)^{-1}$ where $n^{-1}(\partial P/\partial n)^{-1}$ is the isothermal compressibility. The quantity, $(\partial P/\partial\phi)$, represents the effect of slow modes on the local pressure, which accounts for the effect of slow modes in the speed of sound in the system (Appendix C). The asymmetry in $\mathcal{S}_{nn}(\boldsymbol{k},\omega)$ with respect to ω increases with increase in $(\partial P/\partial\phi)$. This is distinctly visible in Fig. 4 in comparison to results displayed in Fig. 1(a).

Figure 5 displays the structure factor with increased ϕ value. The height of the peaks get enhanced significantly for higher values of ϕ. The introduction of slow modes is intended to account for the higher-order gradients (required for system far away from equilibrium) which become relevant at hydrodynamic scales. On the other hand, nonequilibrium fluxes at lower order are also present. The nonequilibrium modes of different orders should be taken into account through slow modes for onset of large fluctuations. For relatively higher fluctuations, even second-order gradients would be accounted through the slow mode, leaving only first-order gradients relevant for fast nonequilibrium modes. On the other hand, for relatively lower fluctuations, the nonhydrodynamic modes at second

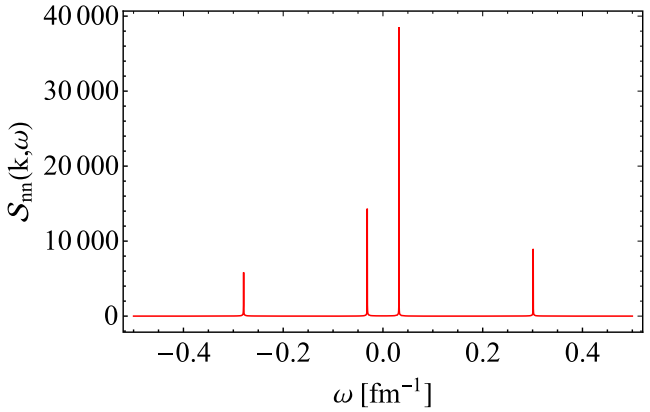

FIG. 5. Variation of $\mathcal{S}_{nn}(\boldsymbol{k},\omega)$ with ω for $k = 0.1$ fm^{-1} and $r = 0.2$; i.e., the system is away from CEP with increased ϕ modes in the system, which increases the thermal fluctuation.

order will be of fast modes, and the interplay of these nonhydrodynamic modes with the slow modes may be understood through the comparison of results with slow modes for first-order theory (where contribution from higher-order derivatives to fast dissipative modes are negligible) and a second-order theory. Moreover, for (nonrelativistic) condensed matter systems where contribution from second-order gradients and couplings can be negligible, it is interesting to know what effect will be there for the slow modes.

In Fig. 6, the structure factor for second-order hydrodynamics has been compared with first-order hydrodynamics (relativistic Navier-Stokes). Interestingly, the structure factor for first-order hydrodynamics admits an R peak at the origin and two symmetric B peaks located on the opposite sides of the R peak. The effects of ϕ seems to be inconsequential in terms of the arising of extra peaks in the first-order theory. The extra peaks do not appear because of the vanishing of the coupling and relaxation coefficients in the first-order hydrodynamics. However, the effect of slow modes in first-order theory is seen in the difference of B-peak heights.

Equations (3) (expression of the energy-momentum tensor) and (16) indicate that the coupling of ϕ enters the system through q^μ. The first-order theory can be obtained from second-order theory by setting the coupling coefficients ($\tilde{\alpha_0}$ and $\tilde{\alpha_1}$) and relaxation coefficients (β_0, $\tilde{\beta_1}$, and β_2) to zero in Eq. (16). Therefore, the only term through which the coupling of ϕ enters the first-order hydrodynamics (Navier-Stokes) is given by the first term of q^μ in Eq. (16), that is, $q^\mu = -\kappa T \Delta^{\mu\nu}[\beta\partial_\nu(T + b\pi)]$. It is interesting to note that the incorporation of ϕ has just shifted the temperature from T to $T + b\pi$ through its chemical potential π. This term does not introduce any ω dependence; therefore, the presence of ϕ in first-order hydrodynamics will not introduce an extra peak.

Until now, it is evident that the extra peaks are originating from coupling of heat flux with the scalar field in second-order theory. However, it is not clear whether the coupling with the longitudinal or transverse modes or both is responsible for these peaks in second-order theory. We verify it by taking only longitudinal modes of second-order theory. The ω dependence of $\mathcal{S}_{nn}(\boldsymbol{k},\omega)$ derived from the longitudinal dispersion relation with and without ϕ has been depicted in Fig. 7. We find that the elastic ($\omega = 0$) R peak is recovered. The widths of the R peak and B peaks are small due to the introduction of the ϕ field (blue dashed line) and closer to the R peak compared to the case when $\phi = 0$. The rate of decay of the thermal fluctuation reflected through the width of the R peak becomes smaller due to the introduction of the field ϕ; that is, the decay of the fluctuation becomes slower in the presence of ϕ.

The comparison of this result with that displayed in Fig. 1(a) indicates that the extra peak appearing in Fig. 1(a) is due to the coupling of the transverse modes with ϕ. It is interesting to note that the extra peak in the dynamic structure factor is caused by the transverse mode in the

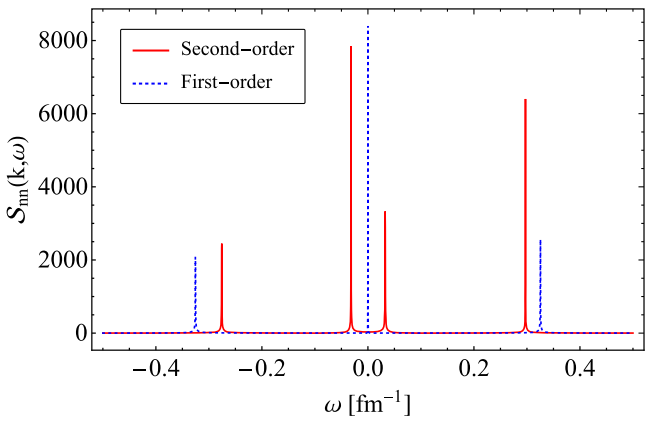

FIG. 6. Variation of $\mathcal{S}_{nn}(\boldsymbol{k},\omega)$ with ω for $k = 0.1$ fm^{-1} and $r = 0.2$. The results for second-order and first-order theories of hydrodynamics are compared here.

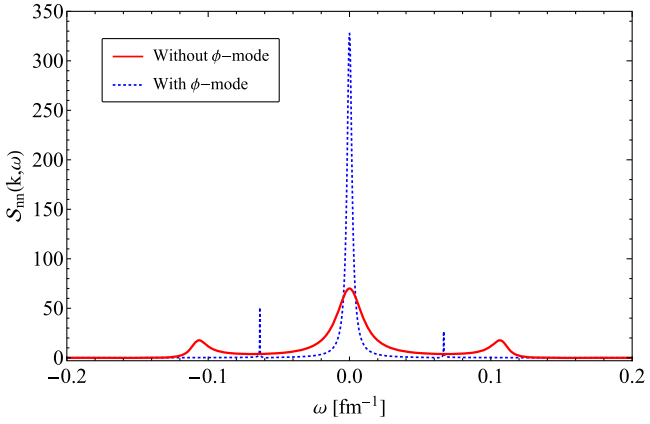

FIG. 7. Variation of $\mathcal{S}_{nn}(\boldsymbol{k},\omega)$ with ω for $k = 0.1$ fm^{-1} and $r = 0.2$ with (dotted line) and without (solid) the ϕ mode, when the longitudinal modes are only considered.

second-order causal hydrodynamics. However, it may create confusion whether the absence of extra peaks at $\phi \neq 0$ is due to the longitudinal modes only or because of first-order hydrodynamics. This can be resolved from the observation that the height asymmetry is different for these two scenarios.

IV. SUMMARY AND DISCUSSIONS

It has been shown in Ref. [17] that the validity of second-order hydrodynamics can be extended near the CEP by introducing an extra slow degree of freedom. Here, we have derived the equation of slow modes for the situation when the extensive nature of thermodynamics is not altered due to the introduction of slow modes. We find that the extensivity condition puts an extra constraint on the coupling of scalar slow modes with the four divergence of velocity. The role of this extra out-of-equilibrium mode on the spectral properties of dynamical density fluctuations near the QCD critical point has been investigated. The dynamical spectral structure $[\mathcal{S}_{nn}(\boldsymbol{k},\omega)]$ in the presence of the out-of equilibrium modes admits four Lorentzian peaks, whereas the dynamic structure factor without slow modes admits three Lorentzian peaks. We find that the asymmetric extra peaks originate due to the coupling of the out-of-equilibrium modes with the hydrodynamic modes. It is also shown that the first-order hydrodynamics is marginally affected by the extra variable introduced to broaden the scope of hydrodynamics. The presence of scalar field introduces the extra peaks in the dynamic structure factor due to the presence of the transverse modes in the causal theory of hydrodynamics. These effects of slow modes on the dynamic structure factor may help in the experimental investigation of the role of slow modes near the $\mathcal{O}(4)$ critical points in condensed matter systems. Consequently, by virtue of universality class, the acquired knowledge on the role of slow modes from experiments on the critical point may be useful in estimating the effect of the CEP through modeling the hydrodynamic evolution of system formed in heavy ion collisions near the QCD critical point. The field representing the OEM, ϕ, plays a crucial role. It reduces the width of the distribution representing the thermal fluctuation, which increases the decay time of the fluctuation.

ACKNOWLEDGMENTS

G. S. and M. H. acknowledge Guruprasad Kadam for fruitful discussions. G. S. also thanks Hiranmaya Mishra for support during part of this work. M. H. would also like to thank Department of Higher Education, Government of West Bengal, India.

APPENDIX A: EXTENSIVITY CONDITION

The infinitesimal change in the total entropy for reversible process of a system of volume V, conserved number $N(=nV)$, slow mode $\Phi(=\phi V)$, and $E(=\epsilon V)$ at temperature T and chemical potential μ is

$$\mathrm{dS} = (E + \mathrm{PdV} - \mu N)/T - \pi d\Phi. \tag{A1}$$

This will give

$$\left.\frac{\partial S}{\partial E}\right|_{N,V,\Phi} = \frac{1}{T}, \qquad \left.\frac{\partial S}{\partial V}\right|_{N,E,\Phi} = \frac{P}{T},$$
$$\left.\frac{\partial S}{\partial N}\right|_{E,V,\Phi} = -\frac{\mu}{T}, \qquad \left.\frac{\partial S}{\partial \Phi}\right|_{E,V,N} = -\frac{\pi}{T}. \tag{A2}$$

The total entropy S satisfies the following relation:

$$S(\lambda E, \lambda V, \lambda N, \lambda\Phi) = \lambda S(E, V, N, \Phi). \tag{A3}$$

Differentiation with respect to λ yields

$$S = E\left.\frac{\partial S}{\partial \lambda E}\right|_{\lambda N,\lambda V,\lambda\Phi} + N\left.\frac{\partial S}{\partial \lambda N}\right|_{\lambda E,\lambda V,\lambda\Phi} + V\left.\frac{\partial S}{\partial \lambda V}\right|_{\lambda N,\lambda E,\lambda\Phi} + \Phi\left.\frac{\partial S}{\partial \lambda \Phi}\right|_{\lambda N,\lambda V,\lambda E}. \tag{A4}$$

Putting $\lambda = 1$ and dividing by V, we get

$$s = \beta(\epsilon + P - \mu n) - \pi\phi, \tag{A5}$$

where $S = sV$ is the entropy density. Equations (A5) and (5) give

$$dP = sdT + nd\mu + \phi d(T\pi). \tag{A6}$$

APPENDIX B: THE SYSTEM OF LINEAR EQUATIONS DERIVED FOR THE PERTURBATIONS IN $\omega - k$ SPACE

The linearized system of equations obtained by using the Fourier-Laplace transformation of the perturbative quantities (generically denoted by δQ) as

$$\delta\tilde{Q}(\boldsymbol{k},\omega) = \int_{-\infty}^{\infty} d^3r \int_0^{\infty} dt e^{-i(\boldsymbol{k}\cdot r+\omega t)}\delta Q(\boldsymbol{r},t) \tag{B1}$$

and

$$\delta\tilde{Q}(\boldsymbol{k},t=0) = \int_{-\infty}^{\infty} d^3r e^{-i(\boldsymbol{k}\cdot r)}\delta Q(\boldsymbol{r},t=0). \tag{B2}$$

The system of equations for the perturbations in hydrodynamic and nonhydrodynamic (ϕ) field in $\omega - k$ space is given below:

$$i\omega\delta\epsilon(\boldsymbol{k},\omega) + ik\delta q_{||}(\boldsymbol{k},\omega) + ik(\epsilon_0 + P_0)\delta u_{||}(\boldsymbol{k},\omega) = -\delta\epsilon(\boldsymbol{k},t=0), \tag{B3}$$

$$\begin{aligned} &i\omega(\epsilon_0 + P_0)\delta u_{||}(\boldsymbol{k},\omega) - ik\delta P(\boldsymbol{k},\omega) - ik\delta\Pi(\boldsymbol{k},\omega) + i\omega\delta q_{||}(\boldsymbol{k},\omega) - ik\delta\pi_{||||}(\boldsymbol{k},\omega) \\ &\quad = (\epsilon_0 + P_0)\delta u_{||}(\boldsymbol{k},t=0) - \delta q_{||}(\boldsymbol{k},t=0), \end{aligned} \tag{B4}$$

$$-i\omega(\epsilon_0 + P_0)\delta u_{\perp}(\boldsymbol{k},\omega) - i\omega\delta q_{\perp}(\boldsymbol{k},\omega) - ik\delta\pi_{\perp||}(\boldsymbol{k},\omega) = (\epsilon_0 + P_0)\delta u_{\perp}(\boldsymbol{k},t=0) - \delta q_{\perp}(\boldsymbol{k},t=0), \tag{B5}$$

$$i\omega\delta n(\boldsymbol{k},\omega) + ikn_0\delta u_{||}(\boldsymbol{k},\omega) = -\delta n(\boldsymbol{k},t=0), \tag{B6}$$

$$\left(1 + i\omega\frac{1}{3}\zeta\beta_0\right)\delta\Pi(\boldsymbol{k},\omega) + ik\frac{1}{3}\zeta\delta u_{||}(\boldsymbol{k},\omega) - ik\frac{1}{3}\zeta\alpha_0\delta q_{||}(\boldsymbol{k},\omega) = -\frac{1}{3}\zeta\beta_0\delta\Pi(\boldsymbol{k},t=0), \tag{B7}$$

$$\begin{aligned} &(1 + i\omega\kappa T_0\beta_1)\delta q_{||}(\boldsymbol{k},\omega) + ik\kappa T_0\delta u_{||}(\boldsymbol{k},\omega) + ik[\kappa - C_{T\pi}K_{q\pi}T_0^2]\delta T(\boldsymbol{k},\omega) - ikT_0^2K_{q\pi}C_{\phi\pi}\delta\phi(\boldsymbol{k},\omega) \\ &\quad - ik\kappa T_0\alpha_0\delta\Pi(\boldsymbol{k},\omega) - ikT_0^2K_{q\pi}C_{n\pi}\delta n(\boldsymbol{k},\omega) - ik\kappa T_0\alpha_1\delta\pi_{||||}(\boldsymbol{k},\omega) \\ &= -\kappa T_0\delta u_{||}(\boldsymbol{k},t=0) - \beta_1\kappa T_0\delta q_{||}(\boldsymbol{k},t=0), \end{aligned} \tag{B8}$$

$$(1 + i\omega\beta_1 kT_0)\delta q_{\perp}(\boldsymbol{k},\omega) + i\kappa T_0(\omega\delta u_{\perp}(\boldsymbol{k},\omega) - k\tilde{\alpha}_1\delta\pi_{\perp||}(\boldsymbol{k},\omega)) = -\kappa T_0[\delta u_{\perp}(\boldsymbol{k},0) - \beta_1\delta q_{\perp}(\boldsymbol{k},t=0)] \tag{B9}$$

$$(1 + 2i\omega\eta\beta_2)\delta\pi_{||||}(\boldsymbol{k},\omega) + ik\frac{4}{3}\eta\delta u_{||}(\boldsymbol{k},\omega) - \frac{4}{3}\delta q_{||}(\boldsymbol{k},\omega) = -2\eta\beta_2\delta\pi_{||||}(\boldsymbol{k},t=0), \tag{B10}$$

$$(1 + 2i\omega\eta\beta_2)\delta\pi_{\perp\perp}(\boldsymbol{k},\omega) - ik\frac{4}{3}\eta\delta u_{||}(\boldsymbol{k},\omega) + ik\frac{4}{3}\eta\tilde{\alpha}_1\delta q_{||}(\boldsymbol{k},\omega) = -2\eta\beta_2\delta\pi_{\perp\perp}(\boldsymbol{k},t=0), \tag{B11}$$

$$(1 + 2i\omega\eta\beta_2)\delta\pi_{\perp\perp}(\boldsymbol{k},\omega) + ik\eta\delta u_{\perp}(\boldsymbol{k},\omega) - ik\delta q_{\perp}(\boldsymbol{k},\omega) = -2\eta\beta_2\delta\pi_{\perp||}(\boldsymbol{k},t=0), \tag{B12}$$

$$\begin{aligned} &\left(i\omega + C_{\phi\pi}\left(\gamma - T_0^2\frac{K_{q\pi}}{\kappa}k^2\right)\right)\delta\phi(\boldsymbol{k},\omega) + \left\{\gamma - K_{q\pi}\left(T_0^2\frac{K_{q\pi}}{\kappa} - \frac{1}{C_{T\pi}}\right)k^2\right\}C_{T\pi}\delta T(\boldsymbol{k},\omega) \\ &\quad + \left(\gamma - T_0^2\frac{K_{q\pi}^2}{\kappa}k^2\right)C_{n\pi}\delta n(\boldsymbol{k},\omega) - ik(\phi - i\omega T_0K_{q\pi})\delta u_{||}(\boldsymbol{k},\omega) \\ &= -\left(1 + ik\frac{K_{q\pi}^2}{\kappa}T_0C_{\phi\pi}\right)\delta\phi(\boldsymbol{k},t=0) - ikT_0K_{q\pi}\delta u_{||}(\boldsymbol{k},t=0), \end{aligned} \tag{B13}$$

where subscripts "||" and "$\perp$" stand for projection along and perpendicular to $\boldsymbol{k}$, respectively. After expressing $\delta\epsilon$ and δp as

$$\delta\epsilon = \left(\frac{\partial\epsilon}{\partial n}\right)\delta n + \left(\frac{\partial\epsilon}{\partial T}\right)\delta T + \left(\frac{\partial\epsilon}{\partial\phi}\right)\delta\phi, \tag{B14}$$

$$\delta P = \left(\frac{\partial P}{\partial n}\right)\delta n + \left(\frac{\partial P}{\partial T}\right)\delta T + \left(\frac{\partial P}{\partial\phi}\right)\delta\phi, \tag{B15}$$

the equations can be arranged to have the matrix from with matrix

$$\mathbb{M}\delta\mathcal{Q} = \mathcal{A} \tag{B16}$$

with

$$\delta\mathcal{Q} = \begin{pmatrix} \delta n \\ \delta T \\ \delta\phi \\ \delta u_{||} \\ \delta q_{||} \\ \delta\pi \\ \delta\pi_{||||} \\ \delta\pi_{\perp\perp} \\ \delta u_{\perp} \\ \delta q_{\perp} \\ \delta\pi_{||\perp} \end{pmatrix}, \qquad \mathcal{A} = \begin{pmatrix} -\delta n(\boldsymbol{k}, t=0) \\ -\epsilon_n \delta n(\boldsymbol{k}, t=0) - \epsilon_\phi \delta\phi(\boldsymbol{k}, t=0) - e_T \delta T(\boldsymbol{k}, t=0) \\ -\delta\phi(\boldsymbol{k}, t=0) - ikT_0 \delta u_{||}(\boldsymbol{k}, t=0)\kappa_{q\pi} \\ (\epsilon_0 + P_0)\delta u_{||}(\boldsymbol{k}, t=0) - \delta q_{||}(\boldsymbol{k}, t=0) \\ -\chi\beta_1 T_0 \delta q_{||}(\boldsymbol{k}, t=0) - T_0\chi\delta u_{||}(\boldsymbol{k}, t=0) \\ -\frac{1}{3}\beta_0\zeta\delta\pi(\boldsymbol{k}, t=0) \\ -2\beta_2\eta\delta\pi_{||||}(\boldsymbol{k}, t=0) \\ -2\beta_2\eta\delta\pi_{\perp\perp}(\boldsymbol{k}, t=0) \\ (\epsilon_0 + P_0)\delta u_{\perp}(\boldsymbol{k}, t=0) - \delta q_{\perp}(\boldsymbol{k}, t=0) \\ -\chi\beta_1 T_0 \delta q_{\perp}(\boldsymbol{k}, t=0) - T_0\chi\delta u_{\perp}(\boldsymbol{k}, t=0) \\ -2\beta_2\eta\delta\pi_{||}\perp(\boldsymbol{k}, t=0) \end{pmatrix} \tag{B17}$$

and

$$\mathbb{M} = \begin{pmatrix} \mathcal{L}_m & \mathbf{0} \\ \mathbf{0} & \mathcal{T}_m \end{pmatrix}, \tag{B18}$$

where

$$\mathcal{L}_m = \begin{pmatrix} i\omega & 0 & 0 & ikn_0 & 0 & 0 & 0 & 0 \\ i\omega\epsilon_n & i\omega\epsilon_T & i\omega\epsilon_\phi & ikw_0 & -ik & 0 & 0 & 0 \\ C_{n\pi}B(k) & C_{T\pi}B(k)+k^2\kappa_{q\pi} & C_{\phi\pi}B(k)+i\omega & ikD_\phi(\omega) & 0 & 0 & 0 & 0 \\ -ikP_n & -ikP_T & -ikP_\phi & -i\omega w_0 & i\omega & -ik & -ik & 0 \\ -ikT_0^2 C_{n\pi}\kappa_{q\pi} & ik(\chi - T_0^2 C_{T\pi}\kappa_{q\pi}) & -ikT_0^2 C_{\phi\pi}\kappa_{q\pi} & iT_0\chi\omega & 1+i\beta_1 T_0\chi\omega & -\chi_T\tilde{\alpha}_0 & -\chi_T\tilde{\alpha}_1 & 0 \\ 0 & 0 & 0 & \frac{i\zeta k}{3} & -\frac{1}{3}i\zeta k\tilde{\alpha}_0 & 1+\frac{1}{3}i\beta_0\zeta\omega & 0 & 0 \\ 0 & 0 & 0 & \frac{4i\eta k}{3} & -\frac{4}{3}i\eta k\tilde{\alpha}_1 & 0 & K(\omega) & 0 \\ 0 & 0 & 0 & -\frac{4}{3}i\eta k & \frac{4}{3}i\eta k\tilde{\alpha}_1 & 0 & 0 & K(\omega) \end{pmatrix}, \tag{B19}$$

where $B(k) = (\gamma - \frac{k^2 T_0^2 \kappa_{q\pi}^2}{\chi})$, $K(\omega) = 1 + 2i\beta_2\eta\omega$, $w_0 = (\epsilon_0 + P_0)$, $D_\phi(\omega) = -(\bar{\phi} - iT_0\omega\kappa_{q\pi}), \chi_T = ikT_0\chi$, and $\mathcal{T}_m$ is given by

$$\mathcal{T}_m = \begin{pmatrix} -i\omega(\epsilon_0 + P_0) & i\omega & -ik \\ iT_0\chi\omega & 1 + i\beta_1 T_0\chi\omega & -ikT_0\chi\tilde{\alpha}_1 \\ i\eta k & -i\eta k\tilde{\alpha}_1 & 1 + 2i\beta_2\eta\omega \end{pmatrix}. \tag{B20}$$

The solution can be written as

$$\delta\mathcal{Q} = \mathbb{M}^{-1}\mathcal{A}. \tag{B21}$$

The solution for fluctuations in net charge (baryon) density is given by

$$\begin{aligned} \delta n(\boldsymbol{k}, \omega) = {} & (-\epsilon_n \mathbb{M}_{12}^{-1} - \mathbb{M}_{11}^{-1})\delta n(\boldsymbol{k}, t=0) + \epsilon_T(-\mathbb{M}_{12}^{-1})\delta T(\boldsymbol{k}, t=0) + (-\epsilon_\phi \mathbb{M}_{12}^{-1} - \mathbb{M}_{13}^{-1})\delta\phi(\boldsymbol{k}, t=0) \\ & + (\epsilon_0 \mathbb{M}_{14}^{-1} - ikT_0 \mathbb{M}_{13}^{-1}\kappa_{q\pi} + \mathbb{M}_{14}^{-1}P_0 - T_0\chi\mathbb{M}_{15}^{-1})\delta u_{||}(\boldsymbol{k}, t=0) \\ & + (-\beta_1 T_0\chi\mathbb{M}_{15}^{-1} - \mathbb{M}_{14}^{-1})\delta q_{||}(\boldsymbol{k}, t=0) + \frac{1}{3}\zeta\mathbb{M}_{16}^{-1}\beta_0\delta\pi(\boldsymbol{k}, t=0) - 2\eta\mathbb{M}_{17}^{-1}\beta_2\delta\pi_{||||}(\boldsymbol{k}, t=0) \\ & - 2\eta\mathbb{M}_{18}^{-1}\beta_2\pi_{\perp\perp}(\boldsymbol{k}, t=0) + (\epsilon_0\mathbb{M}_{19}^{-1} + \mathbb{M}_{19}^{-1}P_0 - T_0\chi\mathbb{M}_{110}^{-1})\delta u_{\perp}(\boldsymbol{k}, t=0) \\ & + (-\beta_1 T_0\chi\mathbb{M}_{110}^{-1} - \mathbb{M}_{19}^{-1})\delta q_{\perp}(\boldsymbol{k}, t=0) - 2\eta\mathbb{M}_{111}^{-1}\beta_2\delta\pi_{||\perp}(\boldsymbol{k}, t=0). \end{aligned} \tag{B22}$$

The elements $\mathbb{M}_{12}$ and $\mathbb{M}_{11}$ can be expressed explicitly as function of frequency and wave vector; thermodynamic quantities temperature, pressure, etc.; and coupling between various hydrodynamic quantities and ϕ. The expressions for $[-\epsilon_n M_{12}^{-1} - M_{11}^{-1}]$ (both for $K_{q\pi} \neq 0$ and $K_{q\pi} = 0$) are given in the supplemental material [66].

APPENDIX C: SPEED OF SOUND AND THE ROOTS OF $\omega(k)$

In this appendix, we provide the expressions for the speed of sound and the roots of $\omega(k)$ with the inclusion of out-of-equilibrium mode ϕ. The speed of sound (c_s) is given by

$$\begin{aligned} c_s^2 &= \left(\frac{\partial p}{\partial \epsilon}\right)_{s/n} \\ &= \frac{sdT + nd\mu + \phi d\pi}{Tds + \mu dn + \pi d\phi} \\ &= \mathcal{A}/\mathcal{B}, \end{aligned} \tag{C1}$$

where $\mathcal{A}$ and $\mathcal{B}$ are given by

$$\mathcal{A} = s + n\mathcal{F} + \phi\mathcal{G}, \tag{C2}$$

$$\begin{aligned} \mathcal{B} = {} & T\left(\frac{\partial s}{\partial T}\right)_{\mu,\pi} + T\mathcal{F}\left(\frac{\partial s}{\partial \mu}\right)_{T,\pi} + T\mathcal{G}\left(\frac{\partial s}{\partial \pi}\right)_{T,\mu} + \mu\left(\frac{\partial n}{\partial T}\right)_{\mu,\pi} + \mu\mathcal{F}\left(\frac{\partial n}{\partial \mu}\right)_{T,\pi} \\ & + \mu\mathcal{G}\left(\frac{\partial n}{\partial \pi}\right)_{T,\mu} + T\left(\frac{\partial s}{\partial T}\right)_{\mu,\pi} + T\mathcal{F}\left(\frac{\partial s}{\partial \mu}\right)_{T,\pi} + T\mathcal{G}\left(\frac{\partial s}{\partial \pi}\right)_{T,\mu}, \end{aligned} \tag{C3}$$

where

$$\mathcal{F} = \frac{[(\frac{\partial s}{\partial T}) - \frac{s}{n}(\frac{\partial n}{\partial T})] + (\frac{\partial \pi}{\partial T})[(\frac{\partial s}{\partial \pi}) - \frac{s}{n}(\frac{\partial n}{\partial \pi})]}{\frac{s}{n}(\frac{\partial n}{\partial \mu})_T - (\frac{\partial s}{\partial \mu})_T}, \tag{C4}$$

$$\mathcal{G} = \frac{[(\frac{\partial s}{\partial T}) - \frac{s}{n}(\frac{\partial n}{\partial T})] + (\frac{\partial \mu}{\partial T})[(\frac{\partial s}{\partial \mu}) - \frac{s}{n}(\frac{\partial n}{\partial \mu})]}{\frac{s}{n}(\frac{\partial n}{\partial \mu})_T - (\frac{\partial s}{\partial \mu})_T}. \tag{C5}$$

The four roots of ω (ω_1, ω_2, and ω_3, and ω_4) indicating the location of peaks in the structure factor obtained from the dispersion relation are given below:

$$\omega_1 = \frac{-\sqrt{-(\epsilon_0 + P_0)^2} + i\epsilon_0 + iP_0}{2T_0\chi} + \frac{\eta k^2\sqrt{-(\epsilon_0 + P_0)^2}}{(\epsilon_0 + P_0)^2} + \mathcal{O}(k^3), \tag{C6}$$

$$\omega_2 = \frac{\sqrt{-(\epsilon_0 + P_0)^2} + i\epsilon_0 + iP_0}{2T_0\chi} - \frac{\eta k^2\sqrt{-(\epsilon_0 + P_0)^2}}{(\epsilon_0 + P_0)^2} + \mathcal{O}(k^3), \tag{C7}$$

$$\begin{aligned} \omega_3 = {} & \frac{i\gamma(C_{\phi\pi}\epsilon_T - C_{T\pi}\epsilon_\phi)}{3\epsilon_T} + \frac{ik^2}{9\epsilon_T(\epsilon_0 + P_0)}[3T_0^2\bar{\phi}C_{\phi\pi}\epsilon_T\kappa_{q\pi} - 3T_0^2\bar{\phi}C_{T\pi}\epsilon_\phi\kappa_{q\pi} + 3\chi\bar{\phi}\epsilon_\phi \\ & - 3T_0^2C_{n\pi}\epsilon_T n_0\kappa_{q\pi} + 3T_0^2C_{T\pi}\epsilon_n n_0\kappa_{q\pi} - 3\chi\epsilon_n n_0 - 3\epsilon_\phi P_0\kappa_{q\pi} - 3\epsilon_0\epsilon_\phi\kappa_{q\pi} - 3T_0\epsilon_\phi P_T\kappa_{q\pi} \\ & + 3T_0\epsilon_T P_\phi\kappa_{q\pi} + \zeta\epsilon_T + 4\eta\epsilon_T + 3T_0\chi P_T] + \mathcal{O}(k^3), \end{aligned} \tag{C8}$$

$$\begin{aligned} \omega_4 = {} & \frac{i\gamma(C_{\phi\pi}\epsilon_T - C_{T\pi}e_\phi)}{3\epsilon_T} + k\sqrt{\frac{\bar{\phi}\epsilon_\phi P_T - \bar{\phi}\epsilon_T P_\phi + \epsilon_T n_0 P_n - \epsilon_n n_0 P_T + \epsilon_0 P_T + P_0 P_T}{\epsilon_T(\epsilon_0 + P_0)}} \\ & + \frac{ik^2}{9\epsilon_T(\epsilon_0 + P_0)}[(3T_0^2\bar{\phi}C_{\phi\pi}\epsilon_T\kappa_{q\pi} - 3T_0^2\bar{\phi}C_{T\pi}\epsilon_\phi\kappa_{q\pi} + 3\chi\bar{\phi}\epsilon_\phi - 3T_0^2C_{n\pi}\epsilon_T n_0\kappa_{q\pi} \\ & + 3T_0^2C_{T\pi}\epsilon_n n_0\kappa_{q\pi} - 3\chi\epsilon_n n_0 - 3\epsilon_\phi P_0\kappa_{q\pi} - 3\epsilon_0\epsilon_\phi\kappa_{q\pi} - 3T_0\epsilon_\phi P_T\kappa_{q\pi} + 3T_0\epsilon_T P_\phi\kappa_{q\pi} \\ & + \zeta\epsilon_T + 4\eta\epsilon_T + 3T_0\chi P_T] + \mathcal{O}(k^3). \end{aligned} \tag{C9}$$

The width of the Brillouin peaks can be identified as

$$\begin{aligned}\Gamma_B = -9\epsilon_T(\epsilon_0+P_0)[&3T_0^2\bar{\phi}C_{\phi\pi}\epsilon_T\kappa_{q\pi} - 3T_0^2\bar{\phi}C_{T\pi}\epsilon_\phi\kappa_{q\pi} + 3\chi\bar{\phi}\epsilon_\phi - 3T_0^2C_{n\pi}\epsilon_T n_0\kappa_{q\pi}\\ &+ 3T_0^2C_{T\pi}\epsilon_n n_0\kappa_{q\pi} - 3\chi\epsilon_n n_0 - 3\epsilon_\phi P_0\kappa_{q\pi} - 3\epsilon_0\epsilon_\phi\kappa_{q\pi} - 3T_0\epsilon_\phi P_T\kappa_{q\pi} + 3T_0\epsilon_T P_\phi\kappa_{q\pi}\\ &+ \zeta\epsilon_T + 4\eta\epsilon_T + 3T_0\chi P_T].\end{aligned} \tag{C10}$$

The speed of sound obtained from the dispersion relation is given by

$$c_s^2 = \frac{\epsilon_T n_0 P_n - \epsilon_n n_0 P_T + \epsilon_0 P_T + P_0 P_T + \bar{\phi}\epsilon_\phi P_T - \bar{\phi}\epsilon_T P_\phi}{\epsilon_T(\epsilon_0+P_0)}. \tag{C11}$$

We have used the following notation in Eqs. (C8)–(C11):

$$X_Y = \left(\frac{\partial X}{\partial Y}\right). \tag{C12}$$

[1] Adam Miklos Halasz, A. D. Jackson, R. E. Shrock, Misha A. Stephanov, and J. J. M. Verbaarschot, On the phase diagram of QCD, Phys. Rev. D **58**, 096007 (1998).

[2] A. Barducci, R. Casalbuoni, G. Pettini, and R. Gatto, Chiral phases of QCD at finite density and temperature, Phys. Rev. D **49**, 426 (1994).

[3] A. Barducci, R. Casalbuoni, S. De Curtis, R. Gatto, and G. Pettini, Pion decay constant at finite temperature and density, Phys. Rev. D **42**, 1757 (1990).

[4] Jürgen Berges and Krishna Rajagopal, Color superconductivity and chiral symmetry restoration at non-zero baryon density and temperature, Nucl. Phys. **B538**, 215 (1999).

[5] O. Kiriyama, M. Maruyama, and F. Takagi, Chiral phase transition at high temperature and density in the QCD-like theory, Phys. Rev. D **62**, 105008 (2000).

[6] Z. Fodor and S. D. Katz, A new method to study lattice QCD at finite temperature and chemical potential, Phys. Lett. B **534**, 87 (2002).

[7] Z. Fodor and S. D. Katz, Critical point of QCD at finite T and μ, lattice results for physical quark masses, J. High Energy Phys. 04 (2004) 050.

[8] M. M. Aggarwal *et al.* (STAR Collaboration), An experimental exploration of the QCD phase diagram: The search for the critical point and the onset of de-confinement, arXiv:1007.2613.

[9] Peter Senger, Heavy-ion collisions at FAIR-NICA energies, Particles **4**, 214 (2021).

[10] Rajiv V. Gavai, QCD critical point: The race is on, Pramana **84**, 757 (2015).

[11] Asakawa Masayuki and Yazaki Koichi, Chiral restoration at finite density and temperature, Nucl. Phys. **A504**, 668 (1989).

[12] A. Barducci, R. Casalbuoni, S. De Curtis, R. Gatto, and G. Pettini, Chiral phase transitions in QCD for finite temperature and density, Phys. Rev. D **41**, 1610 (1990).

[13] Lipei Du, Xin An, and Ulrich Heinz, Baryon transport and the QCD critical point, Phys. Rev. C **104**, 064904 (2021).

[14] Marcus Bleicher and Christoph Herold, Fluid dynamics near the QCD critical point, Proc. Sci. ConfinementX (**2012**) 217 [arXiv:1303.3686].

[15] Carlos Aguiar, Takeshi Kodama, T. Koide, and Y. Hama, Hydrodynamic evolution near QCD critical point, Braz. J. Phys. **37**, 95 (2007).

[16] Chiho Nonaka and Masayuki Asakawa, Hydrodynamical evolution near the QCD critical end point, Phys. Rev. C **71**, 044904 (2005).

[17] M. Stephanov and Y. Yin, Hydrodynamics with parametric slowing down and fluctuations near the critical point, Phys. Rev. D **98**, 036006 (2018).

[18] Masayuki Asakawa, Ulrich Heinz, and Berndt Müller, Fluctuation Probes of Quark Deconfinement, Phys. Rev. Lett. **85**, 2072 (2000).

[19] Sangyong Jeon and Volker Koch, Event-by-event fluctuations, arXiv:hep-ph/0304012.

[20] Volker Koch, Hadronic fluctuations and correlations, arXiv:0810.2520.

[21] Boris Berdnikov and Krishna Rajagopal, Slowing out of equilibrium near the QCD critical point, Phys. Rev. D **61**, 105017 (2000).

[22] H. E. Stanley, *Introduction to Phase Transitions and Critical Phenomena*, International Series of Monographs on Physics (Oxford University Press, Oxford, 1987).

[23] S. K. Ma, *Modern Theory of Critical Phenomena* (Oxford University Press, Oxford, 1976).

[24] L. D. Landau and E. M. Lifshitz, *Fluid Mechanics* (Pergamon, New York, 1959).

[25] W. Israel, Nonstationary irreversible thermodynamics: A causal relativistic theory, Ann. Phys. (N.Y.) **100**, 310 (1976).
[26] Paul Romatschke and Ulrike Romatschke, *Relativistic Fluid Dynamics In and Out of Equilibrium*, Cambridge Monographs on Mathematical Physics (Cambridge University Press, Cambridge, England, 2019).
[27] Marlene Nahrgang, Stefan Leupold, Christoph Herold, and Marcus Bleicher, Nonequilibrium chiral fluid dynamics including dissipation and noise, Phys. Rev. C **84**, 024912 (2011).
[28] Christoph Herold, Marlene Nahrgang, Igor Mishustin, and Marcus Bleicher, Chiral fluid dynamics with explicit propagation of the Polyakov loop, Phys. Rev. C **87**, 014907 (2013).
[29] Krishna Rajagopal, Gregory W. Ridgway, Ryan Weller, and Yi Yin, Understanding the out-of-equilibrium dynamics near a critical point in the QCD phase diagram, Phys. Rev. D **102**, 094025 (2020).
[30] Michal P. Heller and Michal Spalinski, Hydrodynamics Beyond the Gradient Expansion: Resurgence and Resummation, Phys. Rev. Lett. **115**, 072501 (2015).
[31] Paul Romatschke, Relativistic Fluid Dynamics Far From Local Equilibrium, Phys. Rev. Lett. **120**, 012301 (2018).
[32] Michael Strickland, Jorge Noronha, and Gabriel Denicol, Anisotropic nonequilibrium hydrodynamic attractor, Phys. Rev. D **97**, 036020 (2018).
[33] Gabriel S. Denicol and Jorge Noronha, Connecting far-from-equilibrium hydrodynamics to resummed transport coefficients and attractors, Nucl. Phys. **A1005**, 121748 (2021).
[34] Alexander Soloviev, Hydrodynamic attractors in heavy ion collisions: A review, Eur. Phys. J. C **82**, 319 (2022).
[35] Chandrodoy Chattopadhyay, Sunil Jaiswal, Lipei Du, Ulrich Heinz, and Subrata Pal, Non-conformal attractor in boost-invariant plasmas, Phys. Lett. B **824**, 136820 (2022).
[36] Sunil Jaiswal, Chandrodoy Chattopadhyay, Lipei Du, Ulrich Heinz, and Subrata Pal, Nonconformal kinetic theory and hydrodynamics for Bjorken flow, Phys. Rev. C **105**, 024911 (2022).
[37] Michal P. Heller, Alexandre Serantes, Michał Spaliński, Viktor Svensson, and Benjamin Withers, Hydrodynamic Gradient Expansion Diverges beyond Bjorken Flow, Phys. Rev. Lett. **128**, 122302 (2022).
[38] S. K. Ma, *Modern Theory of Critical Phenomena* (Taylor & Francis, London, 2018).
[39] Lindar. E. Reichl, *A Modern Course in Statistical Physics* (Wiley, New York, 2016).
[40] Lars Onsager, Reciprocal relations in irreversible processes. I., Phys. Rev. **37**, 405 (1931).
[41] Lord Rayleigh, X. on the electromagnetic theory of light, London, Edinburgh, Dublin Philos. Mag. J. Sci. **12**, 81 (1881).
[42] Paul A. Fleury and Jean Pierre Boon, Brillouin scattering in simple liquids: Argon and neon, Phys. Rev. **186**, 244 (1969).
[43] Yuki Minami and Teiji Kunihiro, Dynamical density fluctuations around QCD critical point based on dissipative relativistic fluid dynamics -possible fate of mach cone at the critical point-, Prog. Theor. Phys. **122**, 881 (2009).
[44] Md Hasanujjaman, Golam Sarwar, Mahfuzur Rahaman, Abhijit Bhattacharyya, and Jan-e Alam, Dynamical spectral structure of density fluctuation near the QCD critical point, Eur. Phys. J. A **57**, 283 (2021).
[45] Marlene Nahrgang, Marcus Bluhm, Thomas Schaefer, and Steffen A. Bass, Diffusive dynamics of critical fluctuations near the QCD critical point, Phys. Rev. D **99**, 116015 (2019).
[46] Marlene Nahrgang and Marcus Bluhm, Modeling the diffusive dynamics of critical fluctuations near the QCD critical point, Phys. Rev. D **102**, 094017 (2020).
[47] Grégoire Pihan, Marcus Bluhm, Masakiyo Kitazawa, Taklit Sami, and Marlene Nahrgang, Critical net-baryon fluctuations in an expanding system, arXiv:2205.12834.
[48] Kenichi Nagai, Ryuichi Kurita, Koichi Murase, and Tetsufumi Hirano, Causal hydrodynamic fluctuation in Bjorken expansion, Nucl. Phys. **A956**, 781 (2016).
[49] Serguei Chatrchyan *et al.* (CMS Collaboration), Multiplicity and transverse momentum dependence of two- and four-particle correlations in pPb and PbPb collisions, Phys. Lett. B **724**, 213 (2013).
[50] Yi Yin, The QCD critical point hunt: Emergent new ideas and new dynamics, arXiv:1811.06519.
[51] Christoph Herold, Marlene Nahrgang, Yupeng Yan, and Chinorat Kobdaj, Net-baryon number variance and kurtosis within nonequilibrium chiral fluid dynamics, J. Phys. G **41**, 115106 (2014).
[52] J. I. Kapusta, B. Muller, and M. Stephanov, Relativistic theory of hydrodynamic fluctuations with applications to heavy ion collisions, Phys. Rev. C **85**, 054906 (2012).
[53] J. D. Bjorken, Highly relativistic nucleus-nucleus collisions: The central rapidity region, Phys. Rev. D **27**, 140 (1983).
[54] Christoph Herold, Marlene Nahrgang, Yupeng Yan, and Chinorat Kobdaj, Dynamical net-proton fluctuations near a QCD critical point, Phys. Rev. C **93**, 021902 (2016).
[55] Carl Eckart, The thermodynamics of irreversible processes. 3. Relativistic theory of the simple fluid, Phys. Rev. **58**, 919 (1940).
[56] Azwinndini Muronga, Causal theories of dissipative relativistic fluid dynamics for nuclear collisions, Phys. Rev. C **69**, 034903 (2004).
[57] Azwinndini Muronga, Second Order Dissipative Fluid Dynamics for Ultrarelativistic Nuclear Collisions, Phys. Rev. Lett. **88**, 062302 (2002); **89**, 159901(E) (2002).
[58] Pavel Kovtun, Lectures on hydrodynamic fluctuations in relativistic theories, J. Phys. A **45**, 473001 (2012).
[59] Paolo Parotto, Marcus Bluhm, Debora Mroczek, Marlene Nahrgang, J. Noronha-Hostler, Krishna Rajagopal, Claudia Ratti, Thomas Schäfer, and Mikhail Stephanov, QCD equation of state matched to lattice data and exhibiting a critical point singularity, Phys. Rev. C **101**, 034901 (2020).
[60] Md Hasanujjaman, Mahfuzur Rahaman, Abhijit Bhattacharyya, and Jan-e Alam, Dispersion and suppression of sound near the QCD critical point, Phys. Rev. C **102**, 034910 (2020).

[61] Joseph I. Kapusta and Juan M. Torres-Rincon, Thermal conductivity and chiral critical point in heavy ion collisions, Phys. Rev. C **86**, 054911 (2012).
[62] R. Guida and J. Zinn-Justin, 3D Ising model: The scaling equation of state, Nucl. Phys. **B489**, 626 (1997).
[63] Krishna Rajagopal and Frank Wilczek, Static and dynamic critical phenomena at a second order QCD phase transition, Nucl. Phys. **B399**, 395 (1993).
[64] Lord Rayleigh, Lix. on convection currents in a horizontal layer of fluid, when the higher temperature is on the under side, London, Edinburgh, Dublin Philos. Mag. J. Sci. **32**, 529 (1916).
[65] J. M. O. Zarate and J. V. Sengers, *Hydrodynamic Fluctuations in Fluids and Fluid Mixtures* (Elsevier Science, Amsterdam, 2006).
[66] See Supplemental Material at http://link.aps.org/supplemental/10.1103/PhysRevD.106.074029 for the term $[-\in_n M_{12}^{-1} - M_{11}^{-1}]$ which appear as the coefficient of density fluctuation, are given in the supplemental material for $K_{q\pi} \neq 0$ and $K_{q\pi} = 0$.